

The Mid-Infrared Instrument for the James Webb Space Telescope, X. Operations and Data Reduction

Karl D. Gordon^{1,2}, C. H. Chen¹, Rachel E. Anderson¹, Ruymán Azzollini^{3,4}, L. Bergeron¹,
Patrice Bouchet⁵, Jeroen Bouwman⁶, Misty Cracraft¹, Sebastian Fischer^{7,8},
Scott D. Friedman¹, Macarena García-Marín⁸, Alistair Glasse⁹, Adrian M. Glauser¹⁰, G. B.
Goodson¹¹, T. P. Greene¹², Dean C. Hines¹, M. A. Khorrami¹¹, Fred Lahuis^{13,14},
C.-P. Lajoie¹, M. E. Meixner^{1,15}, Jane E. Morrison¹⁶, Brian O’Sullivan¹⁷, K.
M. Pontoppidan¹, M. W. Regan¹, M. E. Ressler¹¹, G. H. Rieke¹⁶, Silvia Scheithauer⁶, Helen
Walker¹⁸, G. S. Wright⁹,

¹Space Telescope Science Institute, 3700 San Martin Drive, Baltimore, MD, 21218, USA

²Sterrenkundig Observatorium, Universiteit Gent, Gent, Belgium

³Dublin Institute for Advanced Studies, School of Cosmic Physics, 31 Fitzwilliam Place, Dublin 2, Ireland

⁴Centro de Astrobiología (INTA-CSIC), Dpto Astrofísica, Carretera de Ajalvir, km 4, 28850 Torrejón de Ardoz, Madrid, Spain

⁵Laboratoire AIM Paris-Saclay, CEA-IRFU/SAP, CNRS, Université Paris Diderot, F-91191 Gif-sur-Yvette, France

⁶Max Planck Institute für Astronomy (MPIA), Königstuhl 17, D-69117 Heidelberg, Germany

⁷Deutsches Zentrum für Luft- und Raumfahrt (DLR), Königswinterer Str. 522-524, 53227, Bonn, Germany

⁸I. Physikalisches Institut. Universität Köln, Zùlpicher Str. 77, 50937, Köln, Germany

⁹UK Astronomy Technology Centre, Royal Observatory, Blackford Hill Edinburgh, EH9 3HJ, Scotland, United Kingdom

¹⁰ETH Zurich, Institute for Astronomy, Wolfgang-Pauli-Str. 27, CH-8093 Zurich, Switzerland

¹¹Jet Propulsion Laboratory, California Institute of Technology, 4800 Oak Grove Drive, Pasadena, CA 91108, USA

¹²Ames Research Center, M.S. 245-6, Moffett Field, CA 94035, USA

¹³Leiden Observatory, Leiden University, PO Box 9513, 2300 RA, Leiden, The Netherlands.

¹⁴SRON Netherlands Institute for Space Research, PO Box 800, 9700AV Groningen, The Netherlands

¹⁵The Johns Hopkins University, Department of Physics and Astronomy, 366 Bloomberg Center, 3400 N. Charles Street, Baltimore, MD 21218, USA

¹⁶Steward Observatory, University of Arizona, Tucson, AZ 85721, USA

¹⁷Airbus Defence and Space, Gunns Wood Road, Stevenage, Hertfordshire, SG1 2AS, UK

¹⁸RALSpace, STFC, Rutherford Appleton Lab., Harwell, Oxford, Didcott OX11 0QX, UK

ABSTRACT

We describe the operations concept and data reduction plan for the Mid-Infrared Instrument (MIRI) for the James Webb Space Telescope (JWST). The overall JWST operations concept is to use Observation Templates (OTs) to provide a straightforward and intuitive way for users to specify observations. MIRI has four OTs that correspond to the four observing modes: 1.) Imaging, 2.) Coronagraphy, 3.) Low Resolution Spectroscopy, and 4.) Medium Resolution Spectroscopy. We outline the user choices and expansion of these choices into detailed instrument operations. The data reduction plans for MIRI are split into three stages, where the specificity of the reduction steps to the observation type increases with stage. The reduction starts with integration ramps: stage 1 yields uncalibrated slope images; stage 2 calibrates the slope images; and then stage 3 combines multiple calibrated slope images into high level data products (e.g. mosaics, spectral cubes, and extracted source information). Finally, we give examples of the data and data products that will be derived from each of the four different OTs.

Subject headings: Astronomical Instrumentation, Data Analysis and Techniques

1. Introduction

The Mid-Infrared Instrument (MIRI) for the James Webb Space Telescope (JWST) will be used for all observations with JWST from 5 to 28.5 μm . MIRI provides observing capabilities for imaging, coronagraphy, low-resolution spectroscopy (LRS) from 5-12 μm , and integral field unit (IFU) medium-resolution spectroscopy (MRS). This paper provides details of the operational model and data reduction plans. Other papers in this series give the science motivation (Rieke et al. 2014a, hereafter Paper I); describe the overall design and construction of the instrument (Wright et al. 2014, hereafter Paper II); and then individually focus on the Imager (Bouchet et al. 2014, hereafter Paper III), the LRS (Kendrew et al. 2014, hereafter Paper IV), the Coronagraphs (Boccaletti et al. 2014, hereafter Paper V), the MRS (Wells et al. 2014, hereafter Paper VI), the detectors (Rieke et al. 2014b, hereafter Paper VII), and the focal plane system (Ressler et al. 2014, hereafter Paper VIII); they are followed by a description of the expected sensitivity and performance (Glasse et al. 2014, hereafter Paper IX).

This paper first describes how users will request observations with MIRI by using Observing Templates (OTs) (§2). The instrument operations that will be driven by the user requests are described in detail. Then the plans for reduction of the MIRI data are given in §3. While the data reduction plans are expected to change at some level as the understanding of the MIRI instrument evolves with continued ground-testing and on orbit observations, the overall plan and many of the details will continue to be as described in this paper. Finally, we show examples of observations for each of the four major MIRI Observation Templates (§4). The overall goal of this paper is to provide an overview of the combined MIRI data acquisition and reduction that are designed to produce high level data products for all MIRI observations. The OTs encode the best data acquisition practices as determined from the instrument experts. The data reduction plan encodes the best practices for producing the highest level data products. This plan is mainly composed of an automated data reduction pipeline with interactive tools provide for the steps that cannot be automated.

2. Observing Templates

The operational model for JWST is to describe the observations using Observation Templates (OTs). The OTs provide a straightforward interface for astronomers to specify the full sequence of steps requested for their programs. The detailed instrument operational commands are directly driven by choices provided in the OTs. The OTs embed the knowledge of instrument experts, effectively exporting their knowledge to all astronomers. The principles that drive the OT design include redundant observations (e.g., multiple dithers), minimizing the use of the instrument mechanisms (e.g., filter and grating wheels), and creating the minimal set of options that accomplishes all expected MIRI science while ensuring robust data reduction and a homogeneous and high-quality archive. This approach has been applied successfully already for the *Infrared Space Observatory* (Kessler et al. 2003), the *Spitzer Space Telescope* (Werner et al. 2004), and the *Herschel Space Observatory* (Pilbratt et al. 2010). In all three cases, OTs were found both to make it straightforward to specify observations and also to increase the probability of obtaining high quality results.

There are four MIRI OTs corresponding to the four main observing modes. These are Imaging, Coronagraphy, Low Resolution Spectroscopy, and Medium Resolution Spectroscopy. The basic parts of a MIRI OT are slewing to the science target, guide star acquisition, target acquisition (if needed), filter/grating moves, taking science exposures, dithering, and mapping (if requested). The full details of the OTs are given in the MIRI Operations

Concept Document¹ and we only provide an overview of the OTs here. While the exact details of the OTs may change before and after the launch of JWST, the overall design should not.

2.1. Guide Star Acquisition

An observational sequence begins with a telescope slew to the target position and acquiring guide star. A guide star acquisition is needed for all observations to provide stable pointing. The Fine Guidance Sensor (FGS) instrument (Doyon et al. 2012) provides the tracking information using known point sources that are mainly from the Guide Star Catalog (Lasker et al. 2008). This catalog has an accuracy of $\sim 0.4''$ (Morrison et al. 2001). For any observations that require placement of a source in an aperture with a higher accuracy, dedicated target acquisition operations are used. The relative astrometric limiting accuracy of the FGS is expected to be ~ 5 milli-arcsec (Chayer et al. 2010) providing sufficient accuracy for all the MIRI apertures using the target acquisition algorithms given in the next subsection. The overall telescope pointing jitter is expected to be similar to the FGS relative astrometric accuracy (Hyde et al. 2004).

2.2. Target Acquisition

Target acquisition (TA) is used to place sources accurately in apertures or subarrays that are small when compared to the 3σ accuracy of the guide stars. The TA is done on-board the JWST spacecraft and this places limitations on the complexity of the algorithms used. For the bright source TA, a clean image of the source is created by taking 4 frames of data in a defined region of the detector, ignoring the 1st frame to avoid detector reset transients, making two estimates of the slope pixel-by-pixel by differencing pairs of frames (i.e. 3-2 and 4-3), and taking the minimum of the two estimates to reject cosmic rays (Gordon et al. 2008). The position of the source in the resulting clean image is determined using a floating centroid algorithm (Meixner et al. 2007). The on-board system uses the measurement of the source position and the known central position of the aperture of interest to perform a small move of the telescope to put the source in the aperture. For faint sources that require longer exposure times to provide the necessary centroiding accuracy, a modified slope creation algorithm is used and the exposure time needed is computed from the flux of the source and the necessary centroiding accuracy (Gordon & Meixner 2008). Three of the standard

¹available in its current version from <http://www.stsci.edu/jwst/instruments/miri/docarchive/>

MIRI imaging filters (F560W, F1000W, and F1500W) and a dedicated neutral density filter allow for TA to be done with blue or red sources and for a range of brightnesses. Filters with central wavelengths longer than $\sim 15 \mu\text{m}$ are not used for TA as the larger size of the diffraction limited MIRI point spread function does not allow for high enough centroiding accuracy (Gordon et al. 2008).

2.3. Visits

An observation consists of a series of observatory and instrument commands. To facilitate efficient scheduling, OT requests are split into a set of Visits. Visits are defined as uninterruptable blocks of commands that carry out the user requested exposures. An observation can be broken into multiple Visits if a new guide star acquisition is needed (e.g. due to a large requested change in the telescope pointing) or if a different instrument mode is used (e.g. changing from MIRI Imaging to MIRI Coronagraphy). As a specific example, the different tiles in a large mosaic are likely to be different Visits, with small scale dithers and exposures with different filters all taking place in a single Visit at each mosaic tile position. Visits are nominally defined such that they do not depend on each other, allowing the scheduling system to interleave Visits from different OTs and/or required instrument or observatory maintenance.

2.4. Special Requirements

There are cases where the ordering or timing of a set of Visits is critical to carrying out the necessary observations. Special Requirements are used to indicate such requests to the schedule system. For example, coronagraphic observations often include measurements of a reference PSF star as well as the target star. These observations should be taken with back-to-back Visits with a Special Requirement to indicate the necessary Visits should be taken without any interruptions.

2.5. Exposures

The MIRI instrument uses 1024×1024 Si:As detector arrays, described in more detail in Papers VII and VIII. For the purposes of MIRI operations, it is useful to know that the detectors are non-destructively read out in equal intervals using four readout channels, until they are reset. A MIRI exposure can consist of multiple integrations where an integration is

defined as the time between subsequent detector resets. The time between successive reads of a pixel is 2.775 s when reading the full detector in the FAST readout mode and 27.75 s in the SLOW readout mode, so the integration times are quantized in these units. Readout patterns suitable to an observation type are specified in the appropriate OT.

2.6. Imaging Observing Template

The full details of the Imager design, build, and ground-testing are given in Paper III. In summary, the MIRI Imager (MIRIM) has 9 wide-band filters with central wavelengths of 5.6, 7.7, 10.0, 11.3, 12.8, 15.0, 18.0, 21.0, and 25.5 μm and a plate scale of $0.11'' \text{ pix}^{-1}$. The MIRIM is critically sampled at 7.0 μm and has an unobstructed FULL array field-of-view (FOV) of $74'' \times 113''$. In addition to the FULL array, MIRIM has four other subarrays that can be used (BRIGHTSKY, SUB256, SUB128, and SUB64); subarrays are required to observe bright targets (e.g. nearby, transiting exo-planet host stars) and might be called upon as a contingency should the telescope thermal emission be unexpectedly high at wavelengths, $\lambda > 20 \mu\text{m}$. The Imaging OT will be used to request all imaging observations, including observations of single fields, mosaicked fields, and non-contiguous fields.

The user options for the Imaging OT are summarized in Table 1. First, the observer selects the full array or a subarray and the dither pattern(s) to use. If the target requires precision synoptic photometry using the SUB64 subarray (e.g., exo-planet transits), then a TA is required to place the target accurately at the center of the subarray. In this case, the observer must specify the TA filter and expected flux in the filter. If the target does not require precision synoptic photometry, then the observer selects a primary and/or a secondary dither pattern.

For full-array imaging, a primary dither pattern moves the target over a significant fraction of the detector area² to mitigate the effects of bad pixels and provide data for self-calibration. The secondary pattern moves the target by a handful of pixels to improve sub-pixel sampling. The dither pattern may be 'Cycling', 'Gaussian', or 'Reuleaux' and can be scaled to have small, medium, or large overall scalings (Chen et al. 2010). For subarray imaging, the dither options depend on the subarray selected so as not to have excursions outside the imaging area. Once the imaging area (array or subarray) and dithering pattern are selected, the observer specifies the imaging filters and their corresponding exposure times. All of the filters selected within a template will be executed with a common subarray and

²The maximum size of the dither pattern that does not require re-acquisition of guide stars is under evaluation.

dither pattern; therefore, the observer must take care to ensure that the selected dither pattern addresses their science goals. For example, the F560W filter is mildly under-sampled with 1.7 pixels per FWHM and observers planning to use PSF reconstruction algorithms should select a secondary dither pattern. However, an observer requesting F560W and F2550W observations together may prefer not to select a secondary dither pattern if PSF reconstruction is not a science driver for their program.

The full sequence of instrument and telescope operations for the Imaging OT is shown in Fig. 1. Note that separate tiles within a mosaic may be considered large moves of the telescope pointing and that such moves are scheduled in separate Visits.

2.7. Coronagraphy Observing Template

MIRI has one Lyot and three 4 quadrant phase mask (4QPM) coronagraphs. The full details of the Coronagraphic design, build, and ground-testing are given in Paper V. The Lyot coronagraph is designed for use with a wide-band filter with a central wavelength of $23\ \mu\text{m}$. The three 4QPM coronagraphs each are designed for a specific wavelength and, thus, are used with medium-band filters with central wavelengths of 10.65, 11.40, and $15.50\ \mu\text{m}$. The FOV of the Lyot coronagraph is $30'' \times 30''$, while the FOVs of the 4QPM coronagraphs are all $24'' \times 24''$. Each coronagraph has a dedicated subarray readout pattern. The Coronagraphy OT will be used for all coronagraphic imaging observations.

The user options for the Coronagraphy OT are summarized in Table 2. The coronagraph to be used is automatically specified by choosing its associated filter. The user must specify the exposure times in each of the requested coronagraphs. All coronagraphic observations require TAs to center the source precisely; the FND filter is a neutral density filter allowing TA on very bright targets. The Lyot and 4QPM coronagraphs have different TA procedures customized for the different coronagraphic types; thus, the user must specify the TA filter and expected flux in the filter for each coronagraph.

Most coronagraphic observations will require reference PSF observations, as the JWST primary mirrors are re-phased periodically and the wavefront errors will change between phasings. The user will specify the same information for the reference source as for the target, except for the choice of coronagraphs. For observations focusing on detecting nearby compact sources, angular differential imaging (ADI, Marois et al. 2006) can be used, where exposures of the source are taken with different telescope roll angles and then subtracted. Such observations can be specified with a Special Requirement. Due to the need to shade the JWST telescope from the Sun, instantaneous roll angles are limited to $\pm 5^\circ$; ADI techniques

used must be consistent with this limitation.

The full sequence of Coronagraphy OT instrument and telescope operations is shown in Fig. 2.

2.8. Low Resolution Spectroscopy Observing Template

The Low Resolution Spectrograph (LRS) provides the capability to take 5-12 μm spectroscopy with a resolution of ~ 100 , using a double prism mounted in the MIRIM filter wheel. The full details of the LRS design, build, and ground-testing are given in Paper IV. The LRS OT will be used to define observations of single sources, either point or extended. The majority of LRS observations are expected to use the $0.51'' \times 4.7''$ slit that includes a filter to block light below 5 μm . For observations desiring the highest accuracy for bright variable sources (e.g. exoplanet transits), there is a slitless mode that avoids variable slit transmission losses. The slitless mode uses the SLITLESSPRISM subarray to allow bright sources to be observed without saturation.

The user options for the LRS OT are summarized in Table 3. LRS observations of point sources will require a TA to place the source accurately to ensure a good wavelength calibration. This TA will be done using the science target. The user picks one of four TA filters and provides an estimate of the flux in this filter. The slit type will be specified as slit or slitless and this decision will automatically select the FULL or SLITLESSPRISM subarray as appropriate. The dither type can be 'None' (e.g. for exoplanet observations), 'Point' where a point source is dithered between positions that are located 1/3 and 2/3 along the slit direction, or 'Extended' where the source is chopped between the center of the slit and a region well outside the slit (Chen et al. 2009). Both the 'Point' and 'Extended' dither patterns provide data to allow the removal of the background. Finally, the user will input the requested exposure time per dither position.

The full sequence of LRS OT instrument and telescope operations is shown in Fig. 3.

2.9. Medium Resolution Spectroscopy Observing Template

The Medium Resolution Spectroscopy (MRS) has four Integral Field Units (IFUs) that feed medium resolution spectrometers operating from 5 to 28.5 μm with a resolution of ~ 3000 . The full details of the MRS design, build, and ground-testing are given in Paper VI. The IFUs are nested, resulting in simultaneous observations in all four spectrometer channels. While this imposes the limitation that the exposures times are the same in all

four channels, it is possible to have different length integrations (see §2.5) between the two short wavelength channel (imaged onto a short wavelength optimized Si:As detector) and two long wavelength channels (imaged onto a different long wavelength optimized Si:As detector). Each IFU has a different FOV ranging from $\sim 3''.7 \times 3''.7$ at the shortest wavelengths to $\sim 7''.7 \times 7''.7$ at the longest wavelengths. Thus, the slice widths and detector plate scales vary with IFU to match the varying diffraction limited PSF of JWST (as discussed in detail in Paper VI).

The MRS OT will be used to take observations of individual and extended sources. The wavelength coverage of each channel of the MRS for a single grating setting is approximately 1/3 of the total wavelength range. Thus, three grating settings (A, B, & C) are required to obtain a full 5-28.5 μm spectrum of a source. Observations with a single grating setting will produce 4 disjoint spectral segments, one from each IFU.

The user options for the MRS OT are summarized in Table 4. A TA will be needed for most MRS observations, requiring the user to specify the TA filter and expected flux in this filter. The user picks whether 1, 2, or all 3 settings are to be utilized. The dither patterns possible are none, 4-point, 6-point, or cycling (Chen et al. 2012). The four IFU slice widths and pixel sizes are optimized to be appropriately sub-sampled by a single 2-point dither pattern for all four IFU channels. Specifically, an offset in the cross-slice direction of $0''.97$ will sub-sample each slice by half a slice width plus an integer number of slices. This is important for the shorter wavelength IFUs as they are undersampled in the cross slice direction. Simultaneously an offset in the along-slice direction by 7.5 pixels ($1''.47$) will subsample the pixels. To mitigate bad pixels, the two point pattern is repeated twice, creating an effective 4-point dither pattern, appropriate for extended sources. For compact sources, where better sampling is needed, a finer 6-point dither is available. Finally, for high-background regions, a self-calibration cycling pattern can be used.

The full sequence of MRS OT instrument and telescope operations is shown in Fig. 4.

3. Data Reduction Plan

The MIRI data reduction plan is based on the extensive testing of the instrument (Paper II), previous work on reducing data from similar instruments and telescopes, and on a series of test campaigns being conducted at JPL using flight-clone detectors and a flight-like data chain. The data reduction is split into 3 stages; an overview is presented in Fig. 5. The 1st stage (CALDETECTOR1) processes the raw data, composed of non-destructively read ramps for each pixel, into an uncalibrated slope image. The 2nd stage (CALIMAGE2 and

CALSPEC2) calibrates each slope image. The 3rd stage (CALIMAGE3, CALCORON3, CALSLIT3, CALSLITLESS3, and CALIFU3) uses the set of slope images taken for an observation and processes them to produce the final data products. The data reduction plan is not restricted to single instances of an OT; observations from multiple instances of OTs can be combined together in the later pipeline stages. Where possible decision points potentially exist (e.g. point or extended source spectral extractions), the philosophy will be to process the observations with both assumptions and provide both to the end user who can then decide which is best for their analysis. A description of each of these stages is given in the following subsections. Some aspects of the data reduction algorithms are expected to change in the coming years as the understanding of the MIRI detectors and instrument improves. However, as this evolution will not be radical, the current plans should continue to provide a valid overview.

3.1. Pipeline Stage One

3.1.1. CALDETECTOR1

The first stage in the pipeline, CALDETECTOR1, is to measure the slope (DN/s units) from the non-destructively read data ramps for each pixel. The data ramps show a number of non-ideal effects common to Si:As devices, including non-linearity, reset anomaly, and latent images, as well as slow drifts in the slopes with amplitudes roughly proportional to the signal level and slow drifts in the zero point of the ramp (see Papers VII and VIII). Here we show two examples. The first is the reset anomaly as shown in Fig. 6, where the first few frames in a dark exposure are lower than expected. The second is non-linearity as shown in Fig. 7, which shows the data ramp for a brightly illuminated pixel that saturates around frame 60. The data values are plotted as plus symbols and a linear fit using the first thirty-five frames is overplotted in blue. The classical non-linearity response of the pixels with increasing signal is shown by the departure of the frame values from the linear line.

Taken all together, these non-ideal detector characteristics pose a challenge to accurate data reduction, since the full suite of issues can be influenced by a large variety of parameters including illumination history, illumination brightness, and time since last exposure. The approach we have adopted is to assume the different detector effects do not depend on each other (e.g. they are orthogonal). This is a standard assumption in most data reduction algorithms, as applied for instruments operating at wavelengths from the ultraviolet to the far-infrared. For example, this assumption has been used successfully for the data reduction of the 24 μm observations taken with the Multiband Imaging Photometer for Spitzer (Gordon et al. 2005). The ordering of the steps that correct the non-ideal characteristics is important

and is done in the reverse of the order that they happen in the detector and electronics. The current steps include 1) rejecting saturated data or bad data based on a predefined bad pixel mask, 2) removing common noise components, 3) correcting for anomalies in the initial frames in an integration caused by the reset, 4) correcting for the contamination of the data by a source from the previous exposure (commonly referred to as persistence), 5) correcting for the non-linearity of the ramps caused by the debiasing of the detectors, 6) subtracting the contribution of the dark current from the ramps, 7) detecting jumps in the ramps caused by cosmic rays and noise spikes (Anderson & Gordon 2011) and, finally, 8) determining the slope of each pixel by fitting line segments to each data ramp. We expect additional steps may be introduced as our understanding of the detectors improves. The ordering of the steps may also change.

3.2. Pipeline Stage Two

The 2nd stage of the pipeline focuses on corrections for pixel- and time-dependent effects on the individual images. Specifically, the corrections are performed on the slope images created by CALDETECTOR1 and produce calibrated images in physical units (e.g., MJy/sr and wavelengths in μm). The reduction splits into two branches with the CALIMAGE2 branch for imaging and coronagraphy and the CALSPEC2 branch for the LRS and MRS spectroscopy.

3.2.1. Common Steps

The first two steps in both branches are the same and are:

Residual Persistence Correction: The main correction for persistent images (also called latents) is done in CALDETECTOR1, but residual persistence will be corrected using measurements of images taken prior to the current image. The persistence signal to subtract will be constructed from the previous images and a persistence model with decay amplitudes and time constants calibrated using dedicated persistence calibration observations.

Flat-Fielding: The variations in sensitivity from pixel-to-pixel will be corrected using flat field images. For MIRIM, it should be possible to generate flat fields from sky signals and standard self-calibration reduction procedures. The uniformity of the Imager response will be determined by dedicated observations of point sources. For the MRS, flat field measurements will utilize the internal flat field source (small spatial scale variations) and external point sources (large spatial scale variations). The flat fields used will be specific to the OT used.

3.2.2. CALIMAGE2

The stage 2 portion of the pipeline for imaging (including coronagraphy) is called CALIMAGE2. The CALIMAGE2 set of algorithms primarily processes single exposure slope images without extensive reference to other slope images taken as part of the OT. The data reduction steps in this stage are similar for the Imaging and Coronagraphic observations, with the main differences being in the calibration files and minor differences in the algorithms for some of the steps. The CALIMAGE2 steps beyond the two already given in §3.2.1 are:

Spatial Mapping: The mapping from pixel to spatial coordinates for each slope image will be computed and associated with each exposure. This provides the information needed to map each pixel to the correct position on the sky. These mappings are mainly based on extensive ground-test distortion measurements and will be confirmed with on-orbit observations.

Absolute Photometric Calibration: The conversion from instrument units (DN/s) to physical units (MJy/sr) is done by multiplying by the appropriate calibration factor. The calibration factors will be derived using Imaging and Coronagraphic observations of flux calibration stars (Gordon et al. 2009; Gordon & Bohlin 2009).

3.2.3. CALSPEC2

The stage 2 portion of the pipeline for spectroscopy is called CALSPEC2. The goal of this stage is to remove additional non-ideal instrumental effects from the slope images for spectroscopic observations. The CALSPEC2 set of algorithms primarily processes single exposure slope images without extensive reference to other slope images taken as part of the OT. The data reduction steps in this stage are similar for the LRS and MRS observations, with the main difference being the calibration files and minor differences in the algorithms for some of the steps. The CALSPEC2 steps beyond the two already given in §3.2.1 are given below in the current planned order.

Straylight Correction: Stray light that contaminates the observed spectra is corrected by subtracting a model of the scattered light. The model for the LRS observations takes into account the light scattered and diffracted from other regions of the detector. For example, the LRS slit observations are measured in a detector region between the regions where the coronagraphic and imaging observations are taken. For the MRS observations, the model

will include the small fraction of the light that is scattered off the optical surfaces and reaches the detectors. Correcting for the extended detector response artifacts between 5 and 8 μm (Paper VII) is under consideration for this stage.

MRS Fringing: The spectral fringing in the MRS observations (Paper VI) will be corrected using a model of the fringes based on ground-testing data and refined using on-orbit data to generate a fringe flat field³.

Spatial and Spectral Mapping: The mapping from pixel to spatial and spectral coordinates for each slope image will be computed and associated with each exposure. This provides the information needed to map each pixel to the correct position on the sky and in wavelength space. These mappings are mainly based on extensive ground-test results and will be confirmed with on-orbit observations. Any variations in the expected centering of point sources in the slit (LRS) or slices (MRS) will be included in the mapping solution.

Absolute Spectrophotometric Calibration: The conversion from instrument units (DN/s) to physical units (MJy/sr) is done by first multiplying by the appropriate Spectral Response Functions (RSRFs) that provide the calibration factor as a function of wavelength (Papers IV and VI). Initial RSRFs have been obtained in ground test and will be refined using LRS and MRS observations of stars. The absolute calibration will be based on standard stars (Gordon et al. 2009; Gordon & Bohlin 2009).

LRS Compact Source Background Subtraction: The background subtraction for LRS exposures for compact sources is straightforward. Compact sources will be noddled/dithered between two different positions in the slit. The background can either be removed by subtracting the two different nod positions, or by using a polynomial fit to regions in the slit with minimal contributions from the source, or by a combination of both approaches. For extended sources, a separate background observation will be used to subtract the background.

LRS Compact Source Extraction: For sources more compact than the LRS slit length, spectra will be extracted using fixed apertures and optimal extraction using a Point Response Function (PRF). The PRF is a slit position dependent table that combines the information on the PSF, the detector sampling, fringing, and the intra-pixel sensitivity variations. For

³An interactive tool will also be provided to assist users in improving the fringe correction beyond that from the pipeline.

the fixed aperture extraction, fringing and intra-pixel corrections are applied to the extracted 1D spectra. For optimal extraction, these corrections are included in the PRF to ensure that low signal-to-noise pixels get low weighting. Observations of point sources through a slit can show variations due to variations in the telescope pointing (e.g. jitter). If the variations are significant, a delta throughput correction will be applied using time resolved telescope pointing information.

3.3. Pipeline Stage Three

The goal of the 3rd stage of the pipeline is to process multiple exposures and extract information for specific sources to produce high quality final data products that are ready for science analysis. This includes combining multiple exposures and extracting source information from the individual and combined exposures. The reduction splits into five branches at this stage. Each of these branches (CALIMAGE3, CALCORON3, CALSLIT3, CALSLITLESS3, and CALIFU3) addresses issues that are specific to the details of the observing mode. Two important concepts for these branches are:

JWST Background: One of the critical steps for most MIRI observations at this stage is to account for the background. The JWST background at MIRI wavelengths will be significant and it is critical to remove and/or model this background to produce high quality reductions. This background is from astrophysical (scattering and emission from Zodiacal and Milky Way dust) and spacecraft (telescope and sunshade) sources, with the former dominating at short wavelengths and the latter dominating at long wavelengths.

Spectral Cubes: One data product that has significant utility for inspection and data analysis of spectral observations, mainly for the MRS IFU spectrometer but also for LRS mapping spectra, is a spectral cube. A spectral cube has the spectral data reprojected from the 2D detector plane to a 3D cube with two spatial and one spectral dimension. The cube is constructed such that each spatial plane is a monochromatic image of the source. The observations that are used to construct the cube can be a single exposure or multiple exposures with different gratings or dither positions.

3.3.1. CALIMAGE3

The 3rd stage of the pipeline for Imaging is called CALIMAGE3. The goal of CALIMAGE3 is the processing of multiple exposures to produce high level imaging products. These

data products are mosaics of multiple individual exposures and catalogs of point sources. The steps in the current planned order are:

Background Matching: The background may change between imaging exposures (particularly if they are not contiguous) due to changes in the telescope emission or zodiacal light. The overlapping regions between successive images will be used to correct for differences in the background between images.

Delta Cosmic Ray Detection: The overlapping regions between any images in the region will be used to detect and reject from further processing residual cosmic rays that were not detected in the ramp processing (see §3.1).

Self Calibration: For observations with sufficient redundancy and appropriate dither patterns, self calibration algorithms (Arendt et al. 2000; Fixsen et al. 2000) will be used to test the dark and flat field frames. If improvements are indicated, the same algorithms will be employed to produce "delta-dark" and "delta-flat" corrections that are correlated with instrumental (not sky) coordinates. The "delta-dark" will include the residual additive instrument signatures (dark and background variations). The "delta-flat" will include multiplicative instrumental signatures (flat field variations).

Source Extraction: Standard PSF fitting algorithms will be used to produce catalogs of point sources to provide at least an initial view of the point sources in the images. The tool that does the source extraction will be available to the user to allow for user interaction to create improved source catalogs.

3.3.2. *CALCORON3*

The 3rd stage of the pipeline for Coronagraphy is called *CALCORON3*. The goal of *CALCORON3* is to combine multiple images of the source and reference star and produce images that suppress/remove the central source PSF as much as possible. The steps in the current planned order are:

Image Coaddition: Multiple images of a source are coadded to produce a high S/N image. The coaddition is done in pixel coordinates as dithering is not possible for coronagraphic observations.

Reference PSF Subtraction: The reference PSF image is subtracted from the science target image. This suppresses the residual speckles and significantly improves the contrast and signal-to-noise of faint sources near the central source. This can be a simple subtraction of a directly observed reference star or a composite reference PSF created from a library of observed reference stars. This composite reference PSF would be created using the LOCI (e.g., Lafreniere et al. 2007), KLIP (e.g., Soummer et al. 2012), ADI (e.g., Lafreniere et al. 2007; Janson et al. 2008), or similar algorithms. The composite reference PSF algorithms directly handle the variations in the source PSF due to changes in the telescope segment phasing and pointing jitter.

3.3.3. CALSLIT3

The 3rd stage of the pipeline for LRS spectroscopy with the LRS slit is called CALSLIT3. The goal of CALSLIT3 is the processing of multiple exposures to produce high level spectral products. The steps are given below, with the differences planned between the extraction of point versus extended sources highlighted.

Compact Sources Combined Spectra: For point sources, the spectra extracted from individual exposures will be coadded to produce a final spectrum of the source. The background subtraction for compact sources is already performed in CALSPEC2.

Extended Source Spectral Cubes: For sources that are extended beyond the slit and have been taken with mapping dither patterns, a spectral cube can be constructed using the known transformation between the detector 2D coordinates to 3D spectral cube coordinates. The tool described in the CALIFU3 section below for extraction of extended sources will be used to extract extended source information for LRS mapping observations.

3.3.4. CALSLITLESS3

The 3rd stage of the pipeline for LRS slitless spectroscopy is called CALSLITLESS3. The slitless mode is designed for high precision observations of variable sources (e.g., exoplanet transients). As the goal of this mode is extreme relative photometric precision, the possible changes in the telescope PSF, fringes, and intra-pixel sensitivity among different exposures during the observation need to be corrected. These corrections will be derived from the observations themselves including the use of a detailed model of the PSF variations.

3.3.5. CALIFU3

The 3rd stage of the pipeline for MRS spectroscopy is called CALIFU3 and has the goal of processing multiple exposures to produce final, high-level products. The steps include background subtraction, creation of spectral cubes, and extraction of sources from the individual exposures and spectral cubes. The CALIFU3 steps in the current planned order are given below.

Background Subtraction: For compact sources with sizes smaller than the offsets between dither positions, the background (and dark current) can be subtracted from one dither position using the other dither positions. For extended sources, either a dedicated off-source observation can be used for background subtraction or, if such observations are not possible, a self-calibration algorithm (Arendt et al. 2000; Fixsen et al. 2000) can be used.

Spectral Cube Construction: The information required to map the detector coordinates to the 3D cube is derived from extensive ground-testing and confirmed on-orbit with mapping observations of a point source. Such cubes will be constructed for individual exposures as well as for the combinations of exposures dithered and with different gratings/channels (e.g., Glauser et al. 2010).

Spectral Extraction: The MRS spectra will be extracted from the individual exposures and spectral cubes. Default extractions assuming a point source and a fully extended source will be provided from the pipeline. A tool that requires user interaction will be provided to allow more sophisticated extractions. One example of such an extraction would be where the variance of the output spectrum is minimized (Horne 1986; Marsh et al. 1989; Robertson 1986).

4. Data and Data Products Examples

Imaging observations of an galaxy are shown in Fig. 8 to illustrate a typical set of Imager data and the corresponding data reduction. The observation sequence includes 12 individual exposures, each taken at a different position in a Reuleaux dither pattern. The full MIRIM footprint is shown in the lower left illustrating that observations are obtained in the Imager, Coronagraphic, and LRS FOVs. For simplicity, only the data taken in the Imager FOV is used to create the final mosaic.

An example of a typical MIRI 4QPM Coronagraphy observing and data reduction se-

quence is shown in Fig. 9. A target object and a reference star are each observed separately with the coronagraph, and then later processed to form the final reference star-subtracted image of the target. The top and bottom sequences represent the separate observations of the target and the reference star. The sequence begins with an observation of the object outside the coronagraph through a TA filter. Once the centroid of the object is obtained, the telescope is offset to place the object in the center of the coronagraph. The correct coronagraphic mask/filter is selected, and exposures are obtained. Typically, multiple exposures of an object are performed to achieve the required signal-to-noise in the scientific region of interest, or to achieve the required signal-to-noise in the diffraction pattern, or both. The multiple exposures are then co-added to form a single image of the target object and the reference star. The final image is formed by subtracting the co-added reference star image from the co-added target star image.

For LRS observations, a common observation set will be noddled observations of a single source. The nods are done at two positions in the slit; the source spectrum can then be extracted directly from the difference image. An example of this type of data, difference image, and extracted spectrum is shown in Fig. 10.

Fig. 11 gives a graphical representation of the construction of the full MRS spectral cube starting with individual detector images. An extended source is observed with the three grating settings to obtain the full spectral coverage in all four IFUs. Such observations will often be taken with 4 dither positions at each grating position, resulting in 24 detector images that are then processed to produce the full wavelength range spectral cube. This full spectral cube can be pictured to be composed of four spectral cubes, one for each IFU.

5. Summary

The current plans for the operations strategy and data reduction for MIRI have been described. The operations strategy centers around the use of Observing Templates to allow astronomers to give only the necessary level of detail to carry out their desired observations. The Observing Templates for MIRI are Imaging, Coronagraphy, Low Resolution Spectroscopy, and Medium Resolution Spectroscopy. The plans for the three stages of MIRI data reduction are outlined. The 1st stage processes the ramps into uncalibrated slopes, then the slopes are calibrated in the 2nd stage, with the final stage focusing on combining individual exposures and extracting source information. The details of the data reduction are expected to evolve as the analysis of ground and commissioning observations improves the understanding of the MIRI detectors and instrument. Finally, we have given examples of the data and data reduction products expected for each of the four MIRI Observation

Templates.

6. Acknowledgments

The work presented is the effort of the entire MIRI team and the enthusiasm within the MIRI partnership is a significant factor in its success. MIRI draws on the scientific and technical expertise many organizations, as summarized in Papers I and II. A portion of this work was carried out at the Jet Propulsion Laboratory, California Institute of Technology, under a contract with the National Aeronautics and Space Administration.

We would like to thank the following National and International Funding Agencies for their support of the MIRI development: NASA; ESA; Belgian Science Policy Office; Centre Nationale D’Etudes Spatiales; Danish National Space Centre; Deutsches Zentrum fur Luft-und Raumfahrt (DLR); Enterprise Ireland; Ministerio De Economía y Competividad; Netherlands Research School for Astronomy (NOVA); Netherlands Organisation for Scientific Research (NWO); Science and Technology Facilities Council; Swiss Space Office; Swedish National Space Board; UK Space Agency.

REFERENCES

- Anderson, R. E., & Gordon, K. D. 2011, PASP, 123, 1237
- Arendt, R. G., Fixsen, D. J., & Moseley, S. H. 2000, ApJ, 536, 500
- Boccaletti, A. et al. 2014, PASP, this volume: **Paper V**
- Bouchet, P. et al. 2014, PASP, this volume: **Paper III**
- Chayer, P., Holfeltz, S., Nelan, E., et al. 2010, Hubble after SM4. Preparing JWST, 59
- Chen, C., Gordon, K. & Watson, D. 2009 The MIRI LRS Dither Pattern JWST-STScI-0001634, STScI
- Chen, C., Anderson, J., Fruchter, A., & Gordon, K. 2010 MIRI Imaging Dither Patterns JWST-STScI-0001657, STScI
- Chen, C. & Glasse, A. 2012 MIRI MRS Dither Patterns JWST-STScI-0001871, STScI
- Doyon, René et al. 2012, SPIE, 8442, 2

- Fixsen, D. J., Moseley, S. H., & Arendt, R. G. 2000, *ApJS*, 128, 651
- Glasse, A. et al. 2014, *PASP*, this volume: **Paper IX**
- Glauser, A. M., Glasse, A., Morrison, J. E., et al. 2010, *Proc. SPIE*, 7731,
- Gordon, K. D., Rieke, G. H., Engelbracht, C. W., et al. 2005, *PASP*, 117, 503
- Gordon, K. 2008, Mid-Infrared Instrument (MIRI) Low Resolution Target Acquisition for Faint Sources, Tech. Rep. JWST-STScI-0001347, STScI
- Gordon, K., & Meixner, M. 2008, Mid-Infrared Instrument (MIRI) Target Acquisition Strategies and Use Cases, Tech. Rep. JWST-STScI-0001407, STScI
- Gordon, K., Bohlin, R., Fullerton, A., Beck, T., & Roberto, M. 2009, JWST Absolute Flux Calibration I. Proposed Primary Calibrators, Tech. Rep. JWST-STScI-0001855, STScI
- Gordon, K. & Bohlin, R. 2009, JWST Absolute Flux Calibration II. Expanded Sample of Primary Calibrators Rep. JWST-STScI-0002540, STScI
- Horne, K. 1986, *PASP*, 98, 609
- Hyde, T. T., Ha, K. Q., Johnston, J. D., Howard, J. M., & Mosier, G. E. 2004, *Proc. SPIE*, 5487, 588
- Janson, M., Reffert, S., Brandner, W., Henning, Th, Lenzen, R., & Hippler, S. 2008, *A&A*, 488, 771
- Kendrew, S. et al. 2014, *PASP*, this volume: **Paper IV**
- Kessler, M. F., Müller, T. G., Leech, K., et al. 2003, *The ISO Handbook*, Volume I - Mission & Satellite Overview
- Lafreniere, D., Marois, C., Doyon, R., Nadeau, D., & Artigau, E. 2007, *ApJ*, 660, 770
- Lasker, B. M., Lattanzi, M. G., McLean, B. J., et al. 2008, *AJ*, 136, 735
- Marois, C., Lafrenière, D., Doyon, R., Macintosh, B., & Nadeau, D. 2006, *ApJ*, 641, 556
- Marsh, T. R. 1989, *PASP*, 101, 1032
- Meixner, M., Cavarroc, C., Regan, M., & Boccaletti, A. 2007, Target Location Algorithms for the Mid-Infrared Instrument (MIRI), Tech. Rep. JWST-STScI-0001134, STScI

- Morrison, J. E., Röser, S., McLean, B., Bucciarelli, B., & Lasker, B. 2001, *AJ*, 121, 1752
- Pilbratt, G. L., Riedinger, J. R., Passvogel, T., et al. 2010, *A&A*, 518, L1
- Ressler, M. et al. 2014, *PASP*, this volume: **Paper VIII**
- Rieke, G. H. et al. 2014b, *PASP*, this volume: **Paper I**
- Rieke, G. H. et al. 2014b, *PASP*, this volume: **Paper VII**
- Robertson, J. G. 1986, *PASP*, 98, 1220
- Soummer, R., Pueyo, L., & Larkin, J. 2012, *ApJL*, 755, 28
- Wells, M. et al. 2014, *PASP*, this volume: **Paper VI**
- Werner, M. W., Rollig, T. L., Low, F. J., et al. 2004, *ApJS*, 154, 1
- Wright, G. S. et al. 2014, *PASP*, this volume: **Paper II**

Table 1. Imaging OT User Options

Question	Choices
Source Coordinates	variety of coordinate systems
TA Filter [†]	F560W, F1000W, F1500W, or FND
TA Flux in Filter [†]	in μJy
Subarray	SUB64, SUB128, SUB256, BRIGHTSKY, or FULL
Dither Pattern	Cycling, Gaussian, Reuleaux, or None
Subpixel Sampling	Yes or No
Filter	F560W, F770W, F1000W, F1130W, F1280W, F1500W, F1800W, F2100W, and/or F2550W
Exposure Time	in seconds

[†]Only required for precision synoptic photometry using the SUB64 subarray.

Table 2. Coronagraphy OT User Options

Question	Choices
Source Coordinates	variety of coordinate systems
TA Filter	F560W, F1000W, F1500W, or FND
TA Flux in Filter	in μJy
Coronagraph/Filter	F1065C, F1140C, F1550C, and/or F2300C
Exposure Time	in seconds
Reference source	all information except choice of coronagraphs

Table 3. LRS Template User Options

Question	Choices
Source Coordinates	variety of coordinate systems
TA Filter	F560W, F1000W, F1500W, or FND
TA Flux in Filter	in μJy
Slit Type	Slit or Slitless
Dither Pattern	Point, Extended, or None
Exposure Time	in seconds

Table 4. MRS template options

Question	Choices
Source Coordinates	RA & DEC
TA Filter	F560W, F1000W, F1500W, or FND
TA Flux in Filter	in μJy
Grating Setting	A, B or C
Dither Pattern	None, 4-point, 6-point, or cycling pattern
Exposure Time	in seconds

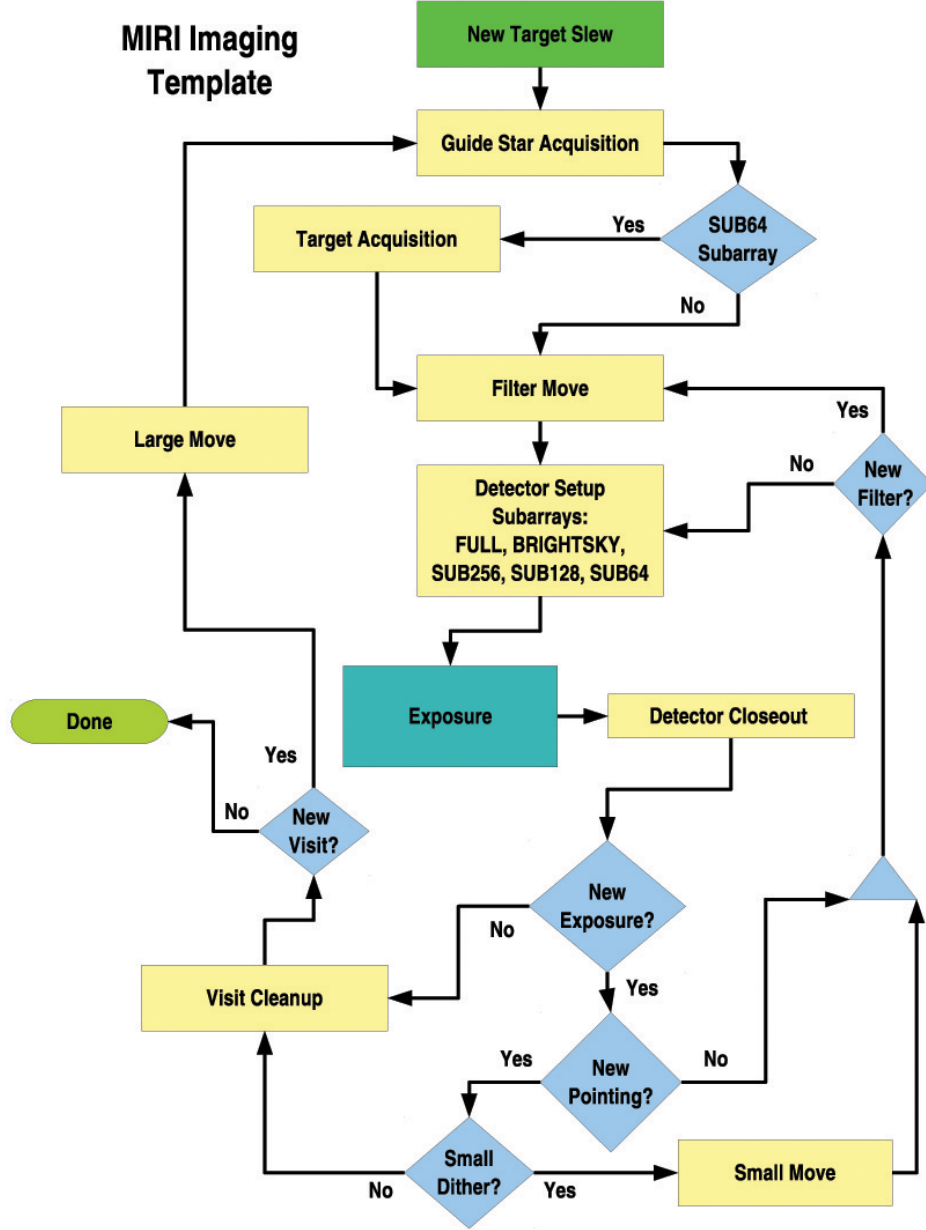


Fig. 1.— The sequence of instrument and telescope operations in the Imaging OT are shown. The main overheads are shown in yellow boxes, decisions in blue boxes, and the actual observations in the “Exposure” box.

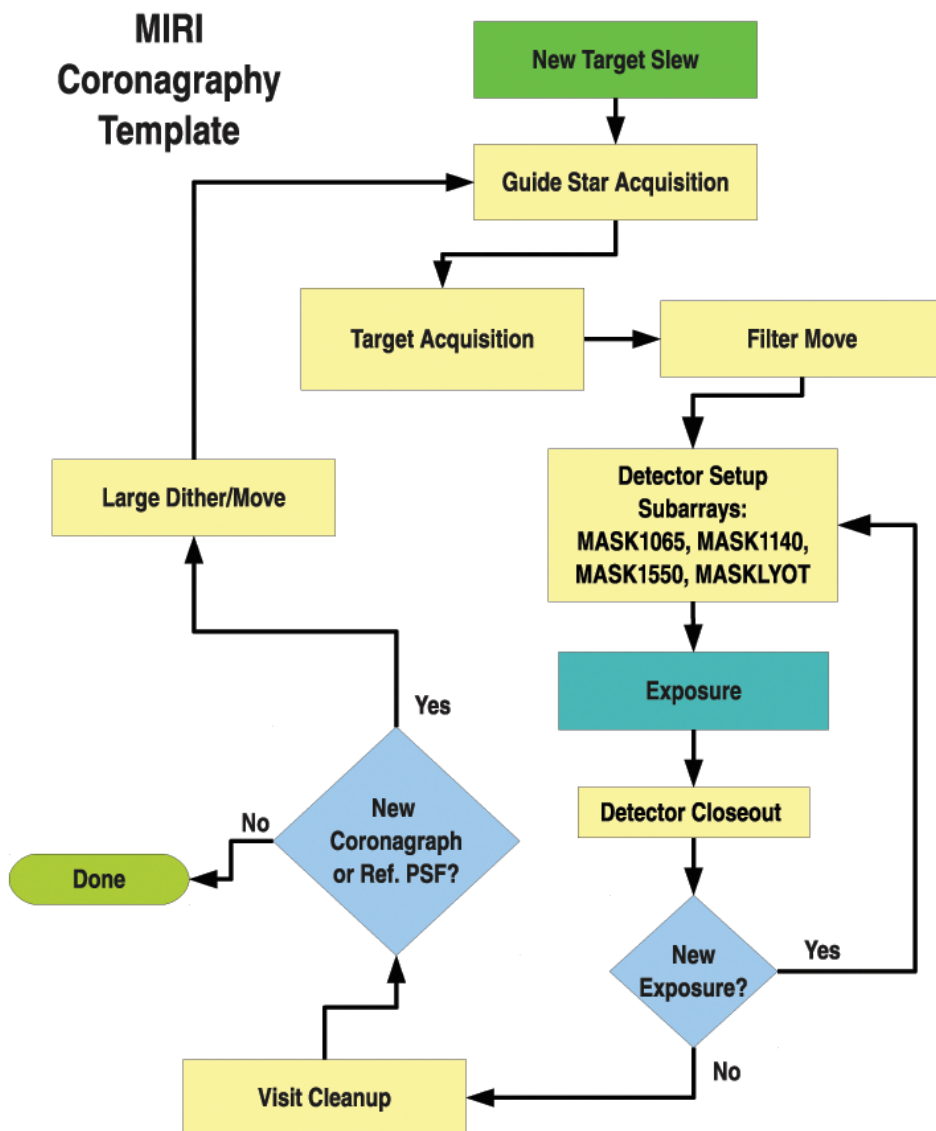
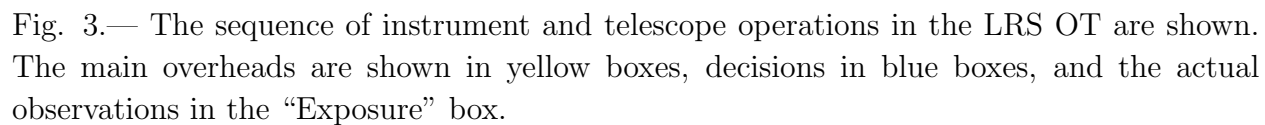


Fig. 2.— The sequence of instrument and telescope operations in the Coronagraphy OT are shown. The main overheads are shown in yellow boxes, decisions in blue boxes, and the actual observations in the “Exposure” box.



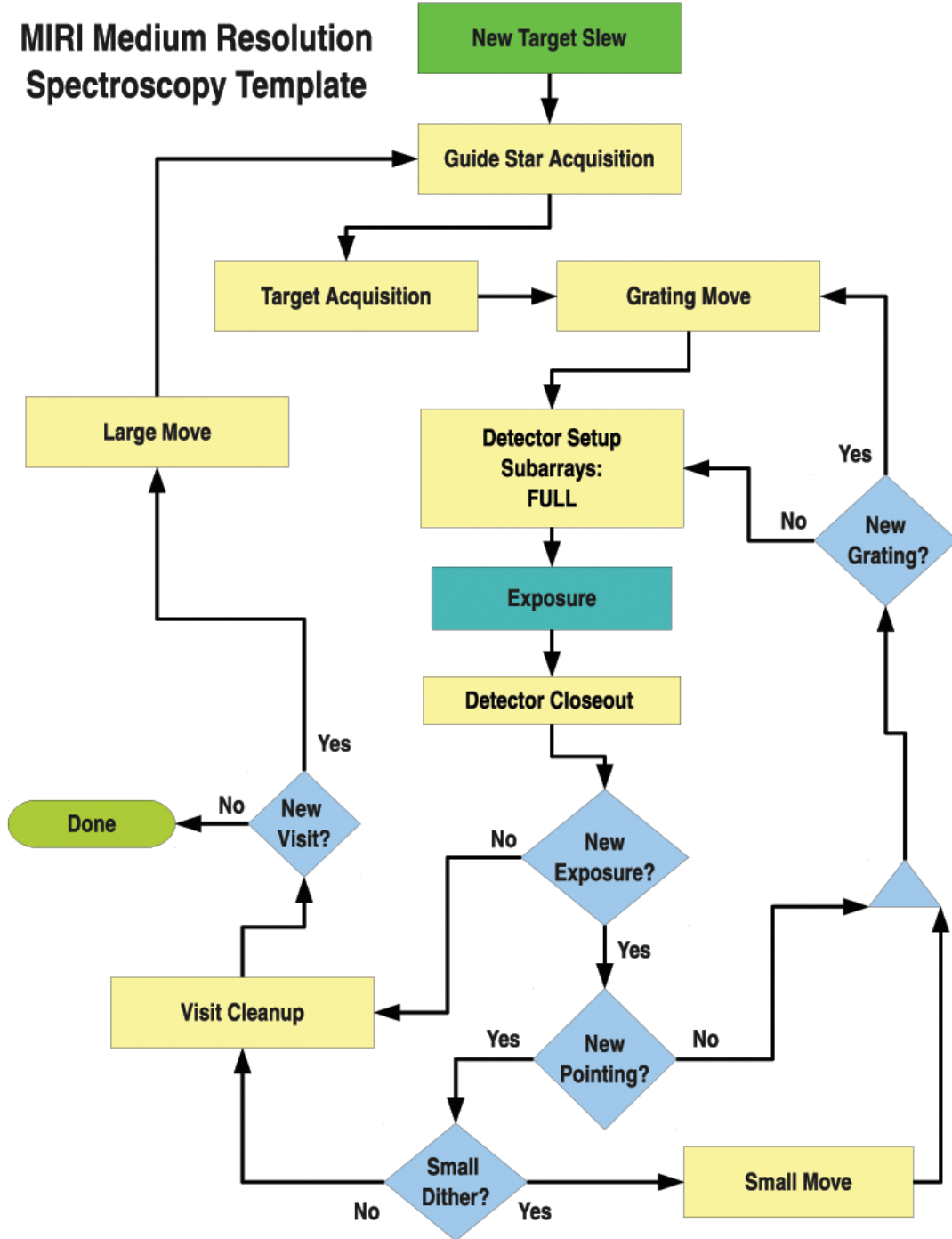


Fig. 4.— The sequence of instrument and telescope operations in the MRS OT are shown. The main overheads are shown in yellow boxes, decisions in blue boxes, and the actual observations in the “Exposure” box.

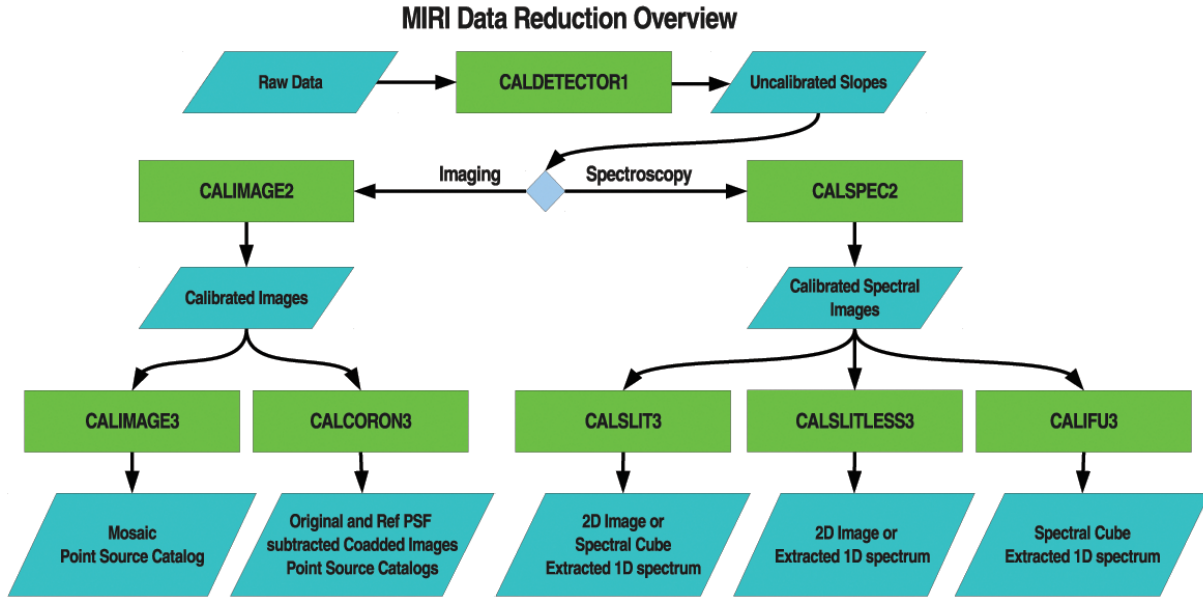


Fig. 5.— The overview of the MIRI data reduction plan.

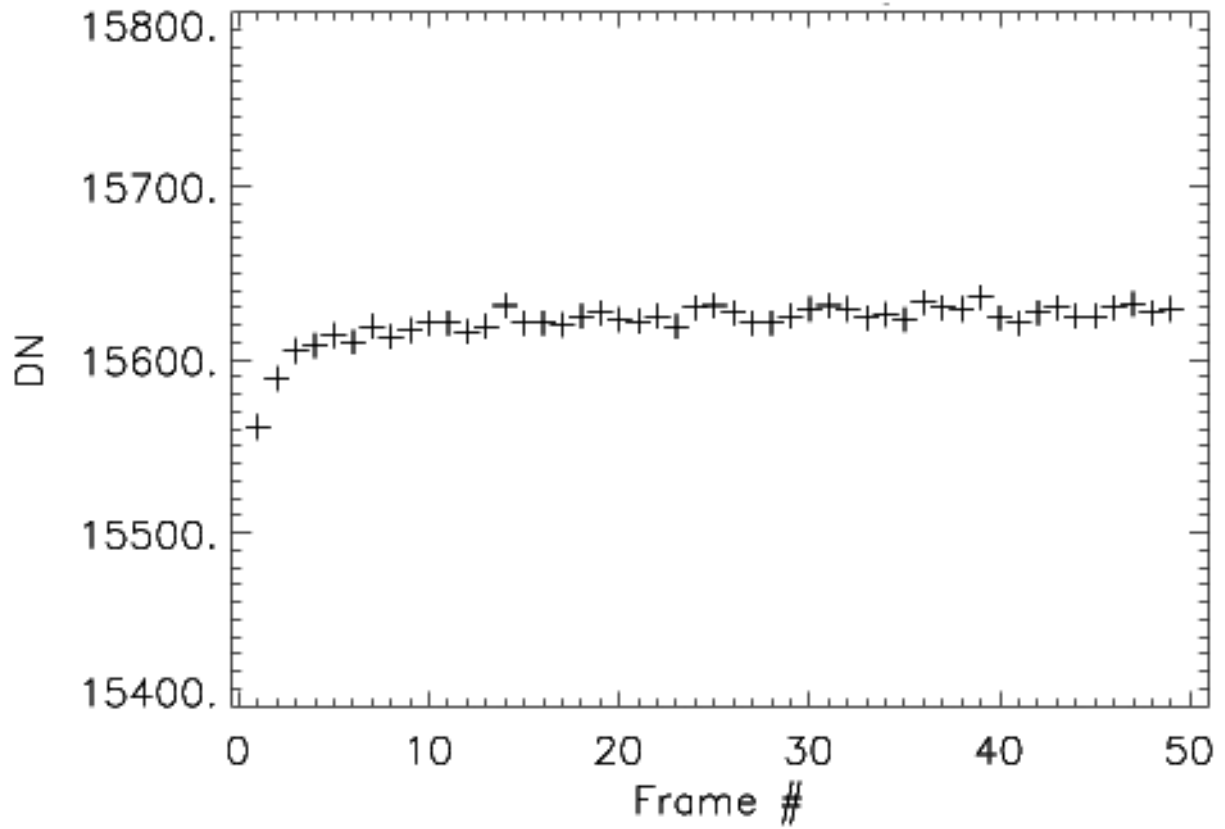


Fig. 6.— A data ramp for a pixel (in DN) is plotted for a dark exposure. The effect of the reset anomaly is shown by the initial frames being offset from their expected values.

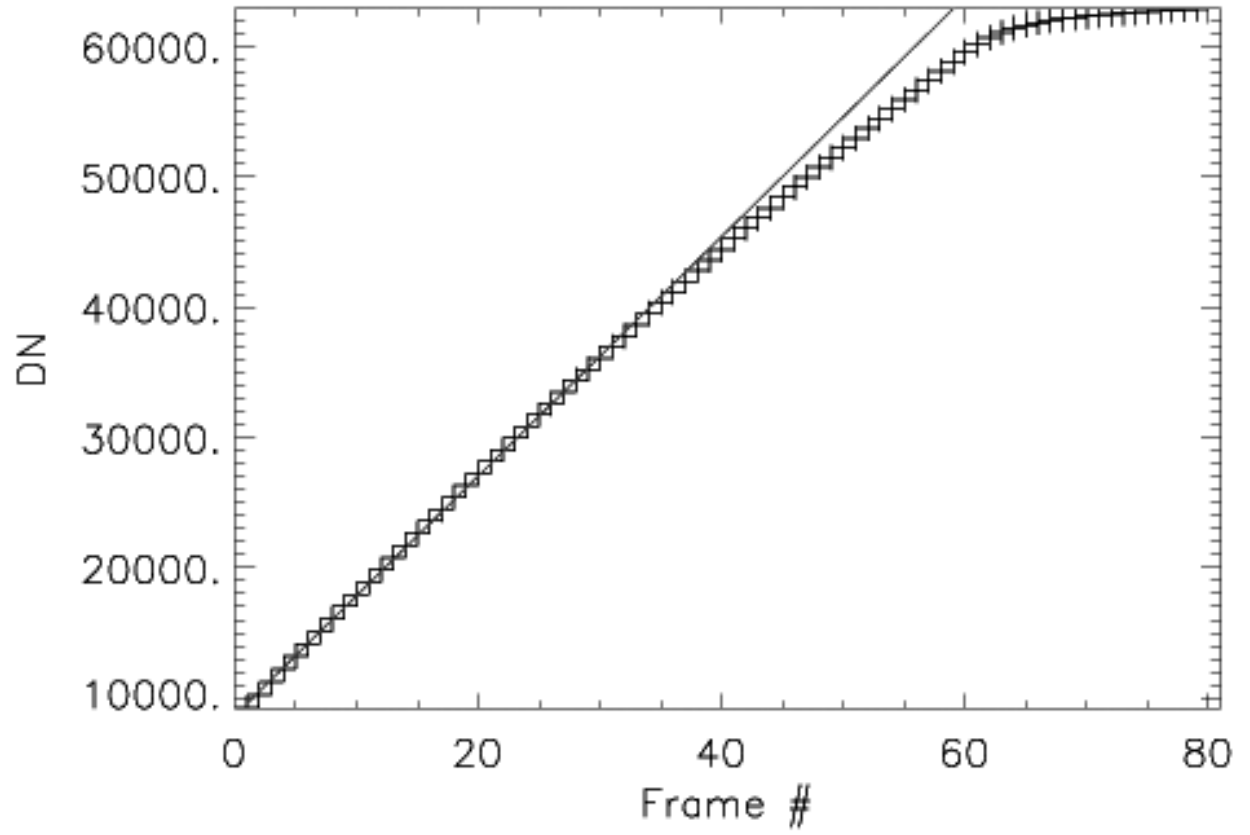


Fig. 7.— An example of a data ramp for a pixel that saturates. A linear fit to the first 35 frames is shown in blue. The reduction in the responsivity with increasing signal is shown by the departure in the frame values from the linear line.

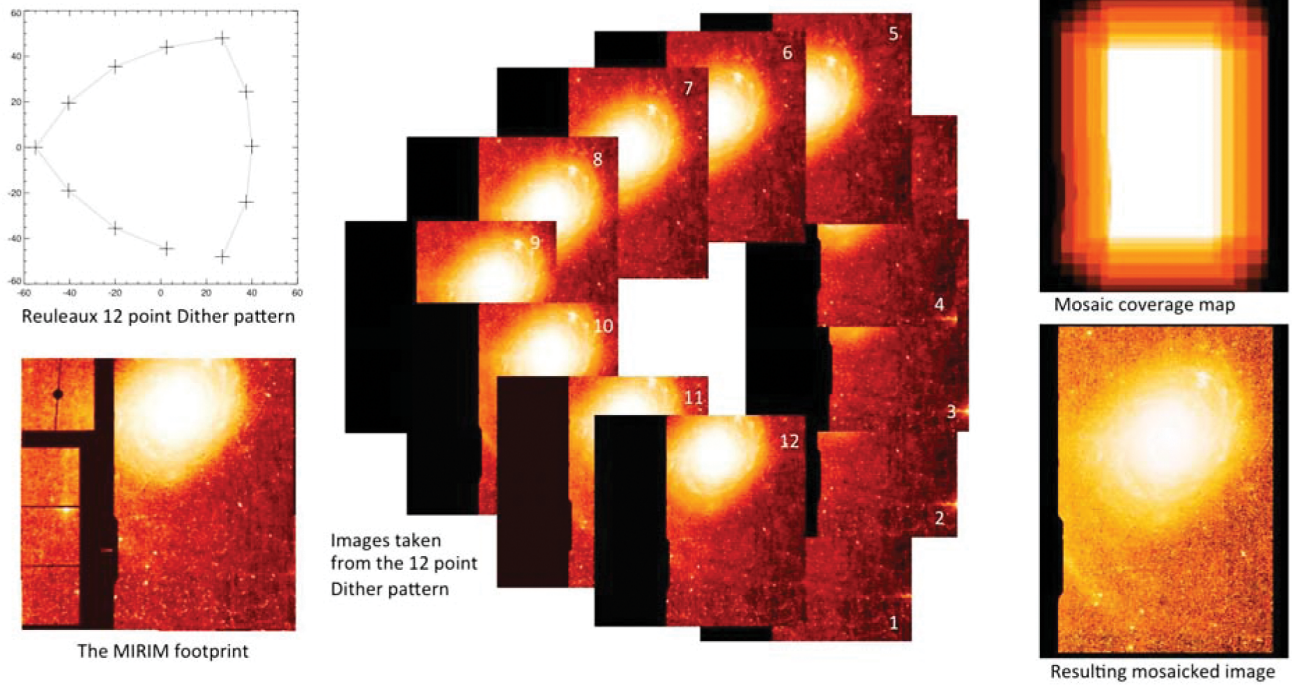


Fig. 8.— An example of imaging observations and data reduction. Twelve images with the 12 point Reuleaux dither pattern are shown separately and combined into a mosaic. The observations taken through the Coronagraphs are not used in the production of the final mosaic for this simulation.

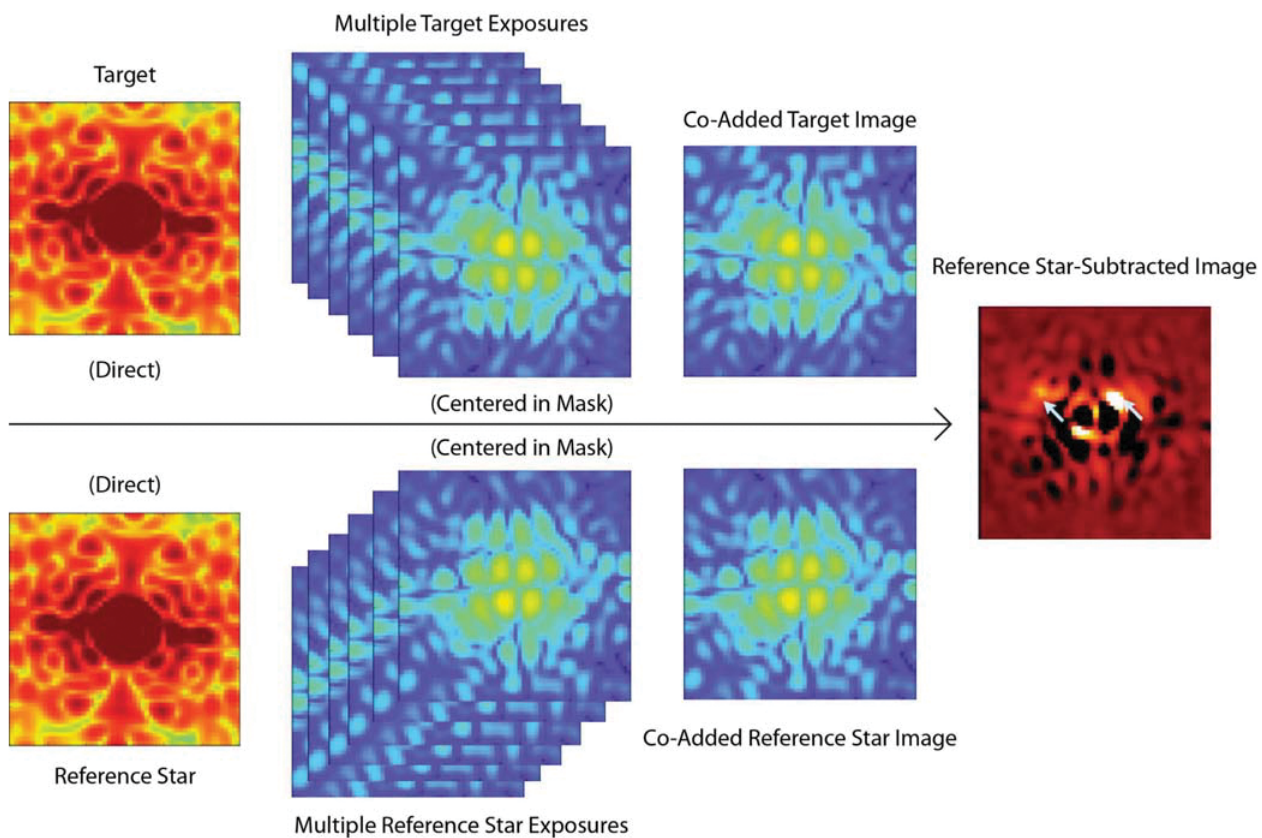


Fig. 9.— An example of Coronagraphic observations and data reduction. Multiple images of the target and reference stars are combined to yield a high quality subtraction of the reference star PSF from that of the target star, revealing faint companions to it.

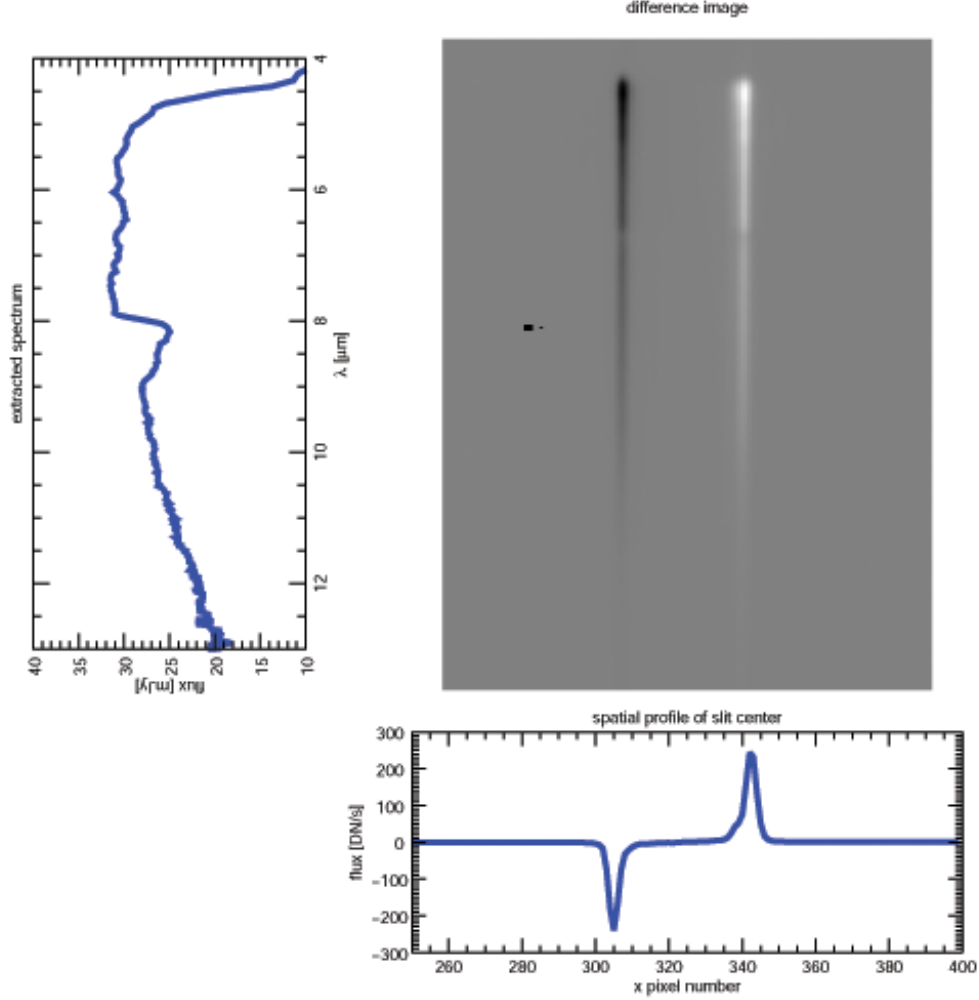


Fig. 10.— An example of LRS data reduction for a point source taken in two different positions in the slit. The difference between the two observations removes the background as shown in the grayscale image. A spatial cut is shown in the lower plot and the extracted spectrum in the left plot. The flux in the spectrum was converted into physical units by using the Relative Spectral Response Function shown in Paper IV.

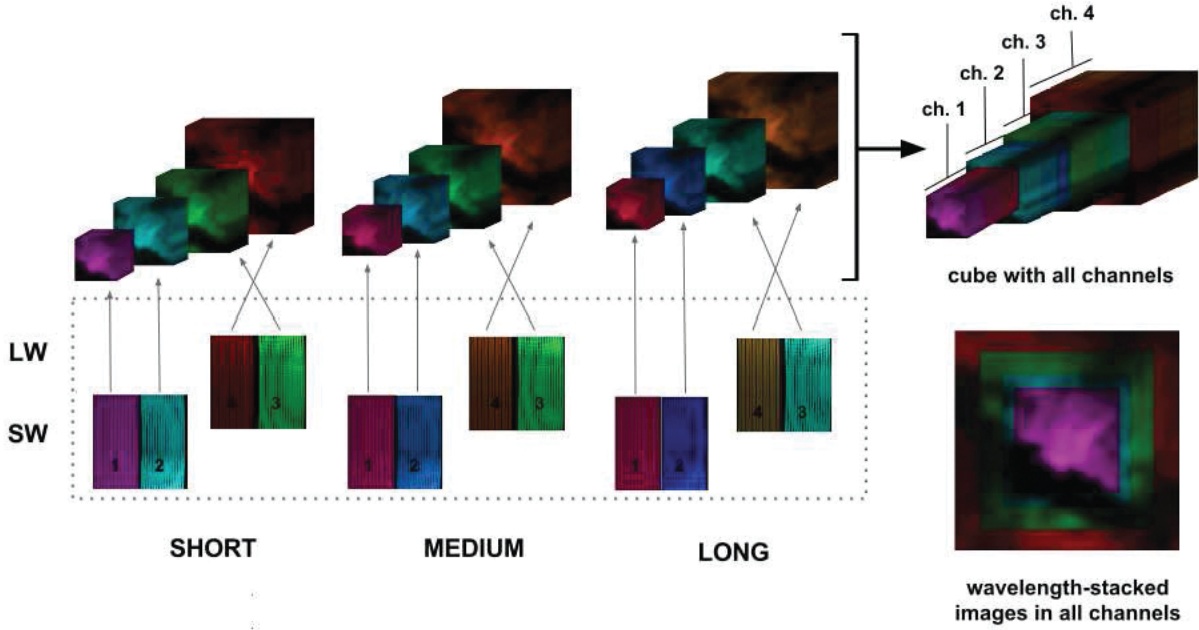


Fig. 11.— An example of the MRS observations that would go into constructing a full spectral cube of a source from 5-28.5 μm . The SW and LW rows give examples of the short and long wavelength detector images. The LONG, MEDIUM, and SHORT columns give the A, B, and C grating settings to obtain full spectral coverage in each of the four IFUs. The detector exposures are color coded by IFU and correspond to the individual IFU spectral cubes (left top row). Finally, the top row, right has a full, merged spectral cube of all four IFUs and the bottom row, right gives a monochromatic image from each IFU illustrating the changing FOV from the shortest to longest wavelength IFU.